applied sciences

MDPI

Article

Identification of Adulterants in Chili Powder Based on the Histogram of Oriented Gradients Algorithm by Using an Electronic Nose

Peng Peng, Fushuai Ba, Yafei Zhang, Feiyang Jiang and Yongli Zhao *

School of Mechanical and Automotive Engineering, Shanghai University of Engineering Science, Shanghai 201620, China
* Correspondence: zyl@sues.edu.cn

Abstract: Driven by economic interests, adding adulterations in chili powder is a problem which threatens people's health. Thanks to its nondestructive, rapid, and portable advantages, electronic nose has more potential to be used for adulteration detection than the traditional methods. An approach for identifying the adulterants in chili powder was proposed in this paper. Firstly, an electronic nose system with 10 gas sensors was designed, and then the response images were drawn based on the response signals of the electronic nose. Afterwards, gas features were extracted from those response images by using a histogram of oriented gradients (HOG) algorithm. Finally, an SVM-based identification model was constructed to achieve the identification of plant adulterants in chili powder. The experimental results showed that the identification accuracy of the adulterant categories (almond shell, red beetroot, and tomato peel) based on the HOG features could reach up to 98.3%, and the identification results for adulterant content were 94.2%, 93.3%, and 95%, respectively. Furthermore, in order to compare the efficiency of the proposed identification approach, the widely used model AlexNet was also investigated and discussed.

Keywords: adulterant identification; pictorial features; electronic nose; histogram of oriented gradients

check for updates

Citation: Peng, P.; Ba, F.; Zhang, Y.; Jiang, F.; Zhao, Y. Identification of Adulterants in Chili Powder Based on the Histogram of Oriented Gradients Algorithm by Using an Electronic Nose. *Appl. Sci.* **2024**, *14*, 1007. https://doi.org/10.3390/app14031007

Academic Editor: Monica Gallo

Received: 13 October 2023
Revised: 28 December 2023
Accepted: 18 January 2024
Published: 24 January 2024

Copyright: © 2024 by the authors. Licensee MDPI, Basel, Switzerland. This article is an open access article distributed under the terms and conditions of the Creative Commons Attribution (CC BY) license (https://creativecommons.org/licenses/by/4.0/).

1. Introduction

Chili powder is a common condiment that many people around the world enjoy eating to enrich the flavor of foods. It is rich in substances such as capsaicin, flavonoids, and phenols [1], which have pharmacological activities and can be used clinically for the prevention and treatment of certain diseases. For example, studies have confirmed that capsaicin has anticancer, antibacterial, analgesic, and cardioprotective effects [2,3]. Compared with bulky foods, powdered foods are much easier for unscrupulous sellers to adulterate in order to reduce the raw material costs. Currently reported adulterants in chili powder mainly include Sudan I–IV dyes [4–7], brick powder [7,8], red beetroot [9,10], almond shell [8,11], dried tomato peel [11], and starch [11]. These adulterants pose significant health risks to consumers. Therefore, it is very important to identify adulterated chili powder.

In recent years, many advanced techniques have been applied in the detection of adulterants. For example, Khan et al. [12] investigated the adulterants in chili powder by using a spectroscopic method. Sarkar et al. [7] used machine-learning algorithms to classify the high-quality images of chili–brick powder adulterants. These methods showed good results in the detection of adulterants. However, the poor portability and the high cost of the spectroscopic equipment significantly limit its practical applications. Dhanya et al. [9] marked plant-based adulterants in chili powder based on PCR (polymerase chain reaction) and SCAR (sequence characterized amplified regions) analyses. This method provided excellent detection accuracy for the adulterations with low concentrations, but it requires complex operating procedures and specialized skills, which makes it unsuitable for rapid detection.

Electronic nose (E-nose) is a system that can detect different odors and identify the chemical components by optimizing its sensor array [13]. It has been widely used in the food industry [14–16]. For example, Liu et al. [17] combined gas chromatography–mass spectrometry with an E-nose to analyze the grinding flavor of pepper and found that the aroma concentration of pepper ground at a low temperature was higher than the traditional milling method. Wen et al. [18] achieved the accurate identification of fruit freshness based on fruity aromas by using E-nose. Heidarbeigi et al. [19] found that the E-nose technique can identify saffron with an adulteration rate higher than 10%. Therefore, as an emerging, rapid, and nondestructive detection method, the E-nose is expected to be suitable for the detection of adulterants in chili powder.

Extracting effective odor features from the response signals and then training models are the two key steps for odor identification by using the E-nose. At present, the commonly used ways to extract the odor features are time-domain features [18,20,21], frequency domain features [22,23], curve fitting [24–26], and data compression [27,28]. However, the effectiveness of the feature-extraction methods is affected by many factors, such as the target gases and the application scenarios. Therefore, it needs to be specially designed for different practical applications [13,29]. In addition, most of the current models used in the E-nose are based on the neural network [30,31]. Although a neural network model can achieve a high identification accuracy, it inevitably takes a relatively long computational time. This shortcoming limits its implementation in rapid identification and its application on portable devices [24,32].

In this paper, an E-nose system was firstly designed and used to detect the botanical adulterants in chili powders. The odor features were then extracted by using the HOG algorithm based on the visualized E-nose response signals. Finally, an identification approach was proposed to identify the different adulterants (almond shell, red beetroot, and tomato peel) and their contents in chili powders. In order to compare the efficiency of the proposed identification approach, the current widely used method AlexNet was also investigated and discussed.

2. Theory and Methodology

Figure 1 illustrates the flow chart of the proposed approach for the identification of adulterants in chili powder. It consists of three main processes: E-nose data acquisition, odor feature extraction, and the adulterant identification model. The odor response data of chili powder containing different adulterants are firstly acquired by using the E-nose system. An odor feature dataset that contributes to the classification and identification of adulterants is then extracted based on the HOG algorithm. Finally, the SVM-based identification model is trained using the constructed dataset to realize the identification of adulterants. Because there is inevitable noise in the E-nose original response signals [13,18,24], in order to facilitate the feature extraction and improve the identification accuracy, noise reduction and filtering is conducted during the data acquisition process.

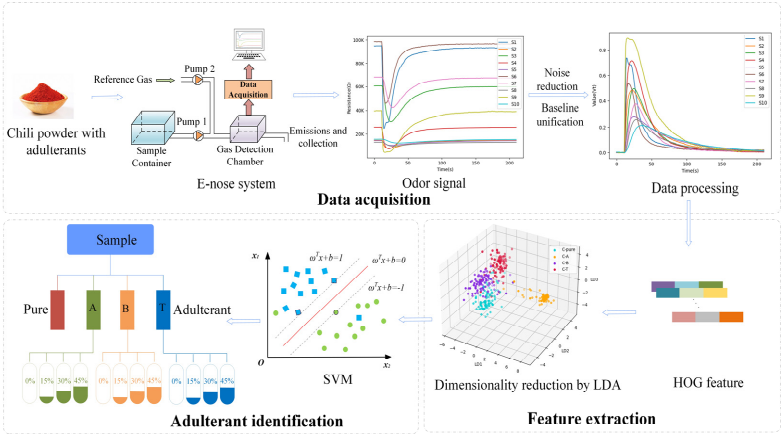


Figure 1. Flowchart of the proposed identification method for chili powder adulterants.

2.1. Odor Feature Extraction Based on HOG

Inspired by the application of image features in computer and engineering science [33,34], this paper proposed an odor feature extraction method based on the HOG algorithm. Firstly, the response images are drawn according to the E-nose response signals, and then the image features are extracted by using the HOG algorithm, as illustrated in Figure 2.

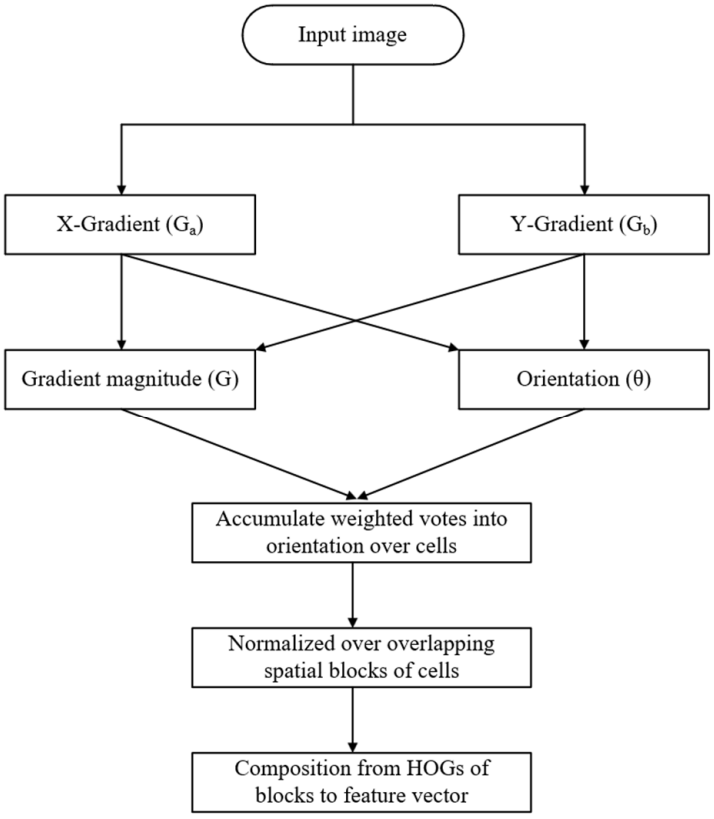


Figure 2. Flowchart for extracting HOG features from images.

Firstly, the horizontal gradient value $G_a(x, y)$ and the vertical gradient value $G_b(x, y)$ are calculated by sliding the discrete derivative mask $[-1, 0, 1]$ and $[-1, 0, 1]^T$ with the following formulas.

$$G_a(x,y) = \frac{\partial I}{\partial x} = I(x+1,y) - I(x-1,y) \quad (1)$$

$$G_b(x,y) = \frac{\partial I}{\partial y} = I(x,y+1) - I(x,y-1) \quad (2)$$

where $I(x, y)$ is the calculated pixel value of the image. The horizontal and vertical gradient values obtained above are then used to calculate the gradient magnitude $G(x, y)$ and gradient direction $\theta(x, y)$ of the image.

$$G(x,y) = \sqrt{G_a(x,y)^2 + G_b(x,y)^2} \quad (3)$$

$$\theta(x,y) = tan^{-1}(\frac{G_a(x,y)}{G_b(x,y)}) \quad (4)$$

After the abovementioned calculation, the image could be divided into small cells with the size of $m \times m$ (m = 4, 6, 8, 10, 12). A local histogram is then created for each cell, which contains 9 bins and its values are distributed between $(0, \pi)$. Weighted voting is subsequently performed on each bin based on the gradient magnitude.

$$\begin{Bmatrix} R_i + G(x,y), & if\ \theta(x,y) = \frac{\pi}{9}i \\ R_i + \left[\frac{\pi}{9}(i+1) - \theta(x,y)\right]G(x,y) \\ R_{i+1} + \left[\theta(x,y) - \frac{\pi}{9}i\right]G(x,y) \end{Bmatrix}, \quad if\ \frac{\pi}{9}i < \theta(x,y) < \frac{\pi}{9}(i+1) \tag{5}$$

where R_i (i = 0, 1, 2, . . ., 8) represents the current value of the ith bin, which is accumulated by iterative weighted voting. Particularly, when the angle is greater than 160°, the corresponding gradient magnitudes will be accumulated in the 0th and 8th bins, respectively.

Finally, we combine $n \times n$ (n = 1, 2, 3, 4) cells to a larger block by sliding windows to overlap 50% of the cells. The L_2-norm is then used to normalize the spliced local histogram and all the normalized results are combined to the final feature vector.

$$V_N = \frac{V_k}{\sqrt{\|V\|^2 + \varepsilon}} \tag{6}$$

where V is the block vector to be normalized, V_k represents the kth element in the block vector V, V_N is the normalized block vector, and ε is a very small amount, which is used to solve the problem with a denominator of zero.

2.2. Feature Dataset Construction

The organizational structure of the odor feature dataset (H) extracted using HOG is shown in Figure 3. In order to balance the sample amount, the 90 pure chili powder samples were randomly divided into three groups. One of the groups was combined with the adulterated almond shell powder samples to construct the feature subsets *H-ca*. The datasets *H-cb* and *H-ct* were built with the same structure as *H-ca*. In order to investigate the difference between the HOG features and the original image features, feature datasets named as *I*, *I-ca*, *I-cb*, and *I-ct* were also built by stitching the pixel values of the image into a one-dimensional feature vector, which also have the same structure as the datasets *H*, *H-ca*, *H-cb*, and *H-ct*.

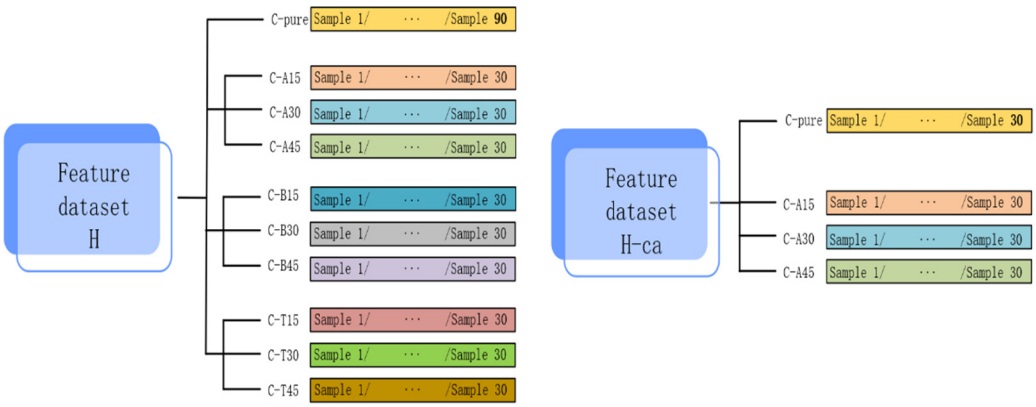


Figure 3. Illustration of the feature dataset structure.

2.3. Identification Model of Adulterants

A support vector machine (SVM) is a supervised machine-learning technique that has been applied to solve a variety of classification and regression tasks. It can distinguish different classes of data by finding a hyperplane in a high-dimensional space [35]. Compared to neural networks, SVM does not need complex network structures and parameters and thus its computation is much faster. SVM has shown positive experimental results in many classification tasks combined with HOG features. The theory of a binary classification support vector machine is as follows:

$$D = \{(x_1, y_1), (x_2, y_2), \ldots, (x_N, y_N)\},\ (i = 1, 2, \ldots, N) \tag{7}$$

D denotes a dataset over the feature space, x_i is the feature vector. y_i represents the category label. The SVM objective function is as follows:

$$\underset{(w,b)}{min} \quad \frac{1}{2}\|\omega\|^2 \tag{8}$$

$$s.t. \quad y_i(\omega \cdot x_i + b) - 1 \geq 0 \tag{9}$$

where ω represents the normal vector to the hyperplane that separates the two different classes, and b is the bias. SVM can solve multiple classification problems by establishing multiple binary classification models. In this paper, the multi-classification SVM model was established based on several 'one-vs-one' models.

3. Experiment

3.1. Materials

According to currently reported adulterants in chili powder and the sensitivity of our home-made sensors, three adulterants, tomato peel powder, red beet root powder, and almond shell powder, were studied in the current work. The raw material chili powder was produced in Nanchong region of China. The three vegetable adulterants (tomato peel powder, red beet root powder, and almond shell powder) were from the regions of Jiaozhou, Changchun, and Chengde of China, respectively. The experimental samples were prepared by adulterating the three adulterants with different mass percentages in the pure chili powder. The content range of the adulterants was set between 0% and 45%. The details of the samples are listed in Table 1.

Table 1. Category and content of adulterant in chili powder.

Sample Name	Chili Powder (wt%)	Adulterant and Its Content (wt%)
C-pure	100	--
C-A15	85	Almond Shell Powder, 15
C-A30	70	Almond Shell Powder, 30
C-A45	55	Almond Shell Powder, 45
C-B15	85	Red Beetroot Powder, 15
C-B30	70	Red Beetroot Powder, 30
C-B45	55	Red Beetroot Powder, 45
C-T15	85	Tomato Peel Powder, 15
C-T30	70	Tomato Peel Powder, 30
C-T45	55	Tomato Peel Powder, 45

3.2. Electronic Nose System

The E-nose system used in this paper is illustrated in Figure 4. The sample container is used to collect sufficient volatile gas of the experimental sample (its material is polyethylene with the capacity of 1 L). The gas detection chamber is employed to place the gas sensor array of the E-nose system (polyethylene, 0.9 L). The diaphragm pumps (Pump 1 and 2) are used to transfer the as-detected odor and the reference gas with a fixed flow rate 1.3 L/min. The whole experiment was carried out under the temperature of 25 $\pm$ 1 °C and humidity 58 $\pm$ 3%, and the laboratory ambient air was used as the reference gas.

The gas sensor array of the E-nose consists of 10 metal oxide semiconductor gas sensors. More details of the material preparation process and the characterization of these gas sensors have been described in the literature [24,36]. When the sensitive material of the sensor is exposed in the detected gas, the change in its resistance value will be converted into the corresponding electrical signal, which is collected by the personal computer with a sampling frequency of 1 Hz. The characteristics of the gas sensors are shown in Table 2.

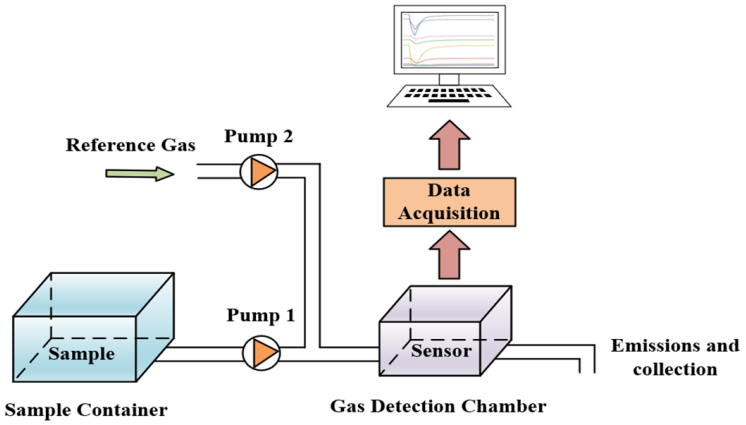


Figure 4. Schematic of the electronic nose system used in the current work.

Table 2. Characteristics of the gas sensors in the E-nose system.

Sensor No.	Main Detected Target Gas
S1	VOCs
S2	Aldehydes, hydrogen sulfide
S3	VOCs, carbon monoxide, ammonia
S4	Benzene, methylbenzene, ethylene
S5	Aldehydes, olefin
S6	Air quality control, acetic acid, acetone
S7	Alkane, ethanol, acetone
S8	Aldehydes, ethylbenzene, methane
S9	Air quality control, hydrogen
S10	Ethanol, ammonia, hydrogen sulfide

3.3. Experimental Procedure

The whole experiment involved nine categories of adulterated samples (three adulterants with three different mass percentages). In total, 30 gas data were randomly collected for each category of sample using the E-nose. In order to balance the sample number for the qualitative analysis, 90 gas data were collected for the pure chili sample. Therefore, a total of 360 sample data were detected during the whole experiment. The details of the odor data collection steps are as follows:

(i) Randomly select one sample, put it in the sample container, and wait 2 min to allow its gas to emit and fill the container;
(ii) Turn on Pump 1 to transfer the sample odor into the gas detection chamber, and the pumping time is set as 10 s;
(iii) Turn on Pump 2 to introduce ambient gas into the gas detection chamber for cleaning. After all the gas sensors return to their initial states, the detection of the next sample can be started.

4. Results

4.1. E-Nose Response Signal

Figure 5 shows the original E-nose response signals of different categories of samples. Before the sample odor is introduced (0~10 s), as all the sensors are exposed in the ambient air at this time, they are in their stable state. When pumping the sample odor into the detection chamber (10~20 s), the resistance values of the gas sensors drop down quickly. After the sample odor is cut off and the ambient gas is subsequently flushed into the detection chamber (20~210 s), all the gas sensors could gradually return back to their initial state. Those response behaviors indicated that the E-nose has a good sensitivity and desorption ability for the experimental gases.

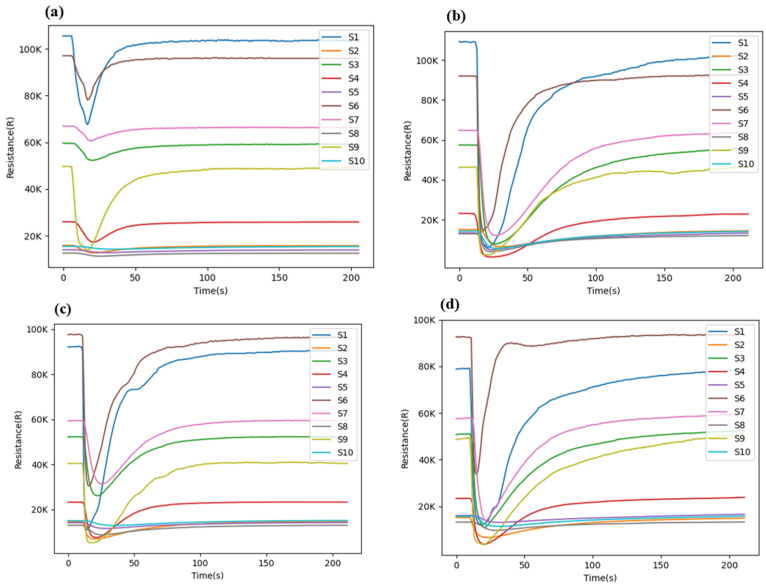


Figure 5. The E-nose original response signal of different categories of samples: (**a**) C-pure; (**b**) C-A15; (**c**) C-B15; (**d**) C-T15.

4.2. Signal Pre-Processing

Due to the difference in the sensitive materials, different sensors will have different response sensitivities to the same circumstance. The influence of environmental factors such as temperature and humidity will cause a baseline fluctuation of the sensors [37]. In order to eliminate these effects, we performed the following processing on the original signal data:

$$V_t = \frac{R_0 - R_t}{R_0} \tag{10}$$

where V_t is the real-time response sensitivity of the gas sensor, R_0 represents the resistance value of the sensor in the ambient air, and R_t is the real-time resistance value in the detected gas. The response sensitivity curves of the E-nose calculated according to Equation (10) are shown in Figure 6.

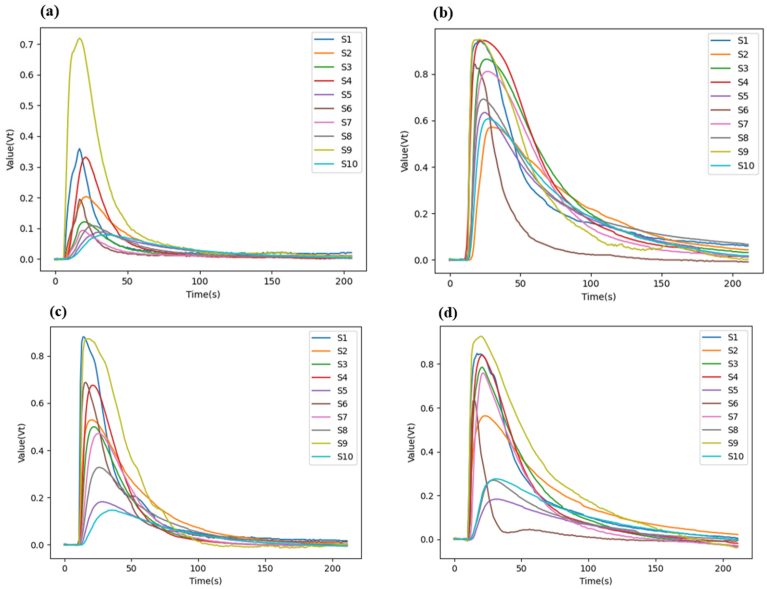


Figure 6. Pre-processed E-nose response data on different categories of samples according to Equation (10): (**a**) C-pure; (**b**) C-A15; (**c**) C-B15; (**d**) C-T15.

5. Discussion

5.1. Comparison of Different Odor Features

After the data pre-processing, odor features were extracted by using the as-proposed HOG algorithm. In order to compare the efficiency of the HOG extraction method, the original response data and images were also directedly used as odor features for the adulterant identification. As the three types of feature datasets are high-dimensional, their dimensions were reduced by using the same method of linear discriminant analysis (LDA) before employing them to train the identification model. LDA is a supervised approach for dimensionality reduction, which is realized by minimizing the intra-class variance and maximining the inter-class variance in a low-dimensional space [38]. It has been successfully applied in gas identification and classification with good results [39,40].

Figures 7–9 show the visualized comparison results of sample distribution after the dimensionality reduction by using LDA on different odor feature datasets. It can be seen that all the feature datasets, the original response data feature, the response image feature, and the HOG feature, can obtain a certain extent of sample dispersion. This indicates the different adulterant categories are discriminable according to the extracted odor features. Furthermore, the HOG feature has an obvious better classification effect than other two types of feature datasets (see Figures 7a, 8a and 9a). For the classification of the adulterant contents, although these three types of feature datasets do not have the same good results as those of the adulterant categories, they still show a certain degree of separation. In addition, the HOG feature also displayed a more obvious clustering effect than the features extracted from the original response data and images, although there is a small amount of overlap between the samples with different adulterant contents.

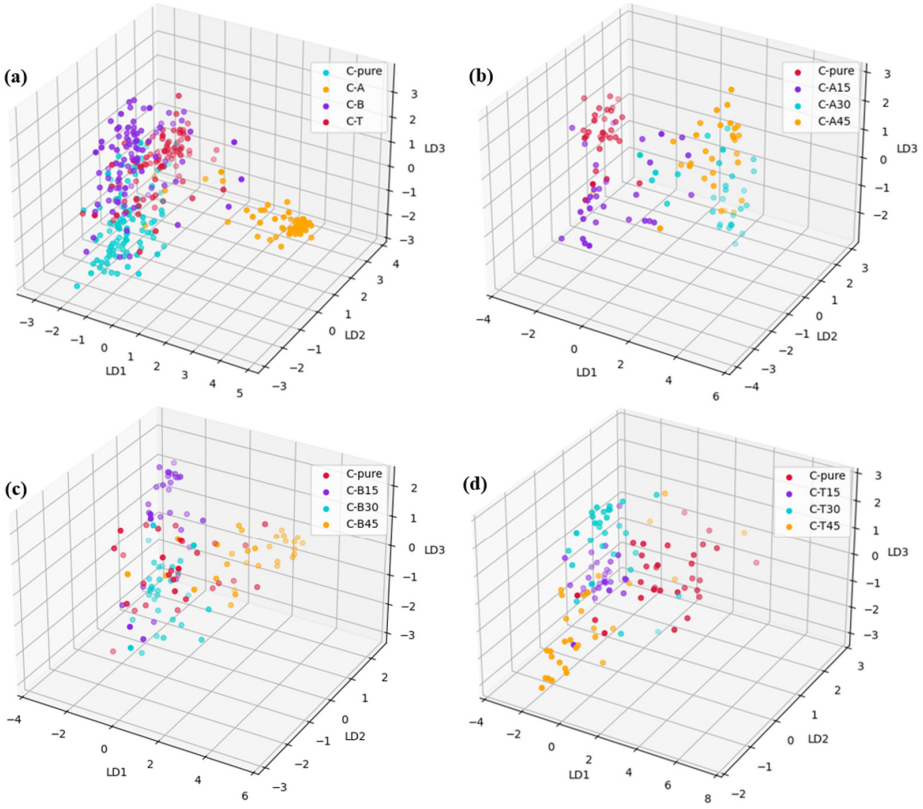


Figure 7. LDA results for different feature datasets extracted from the original response data: (**a**) *D*; (**b**) *D-ca*; (**c**) *D-cb*; (**d**) *D-ct*.

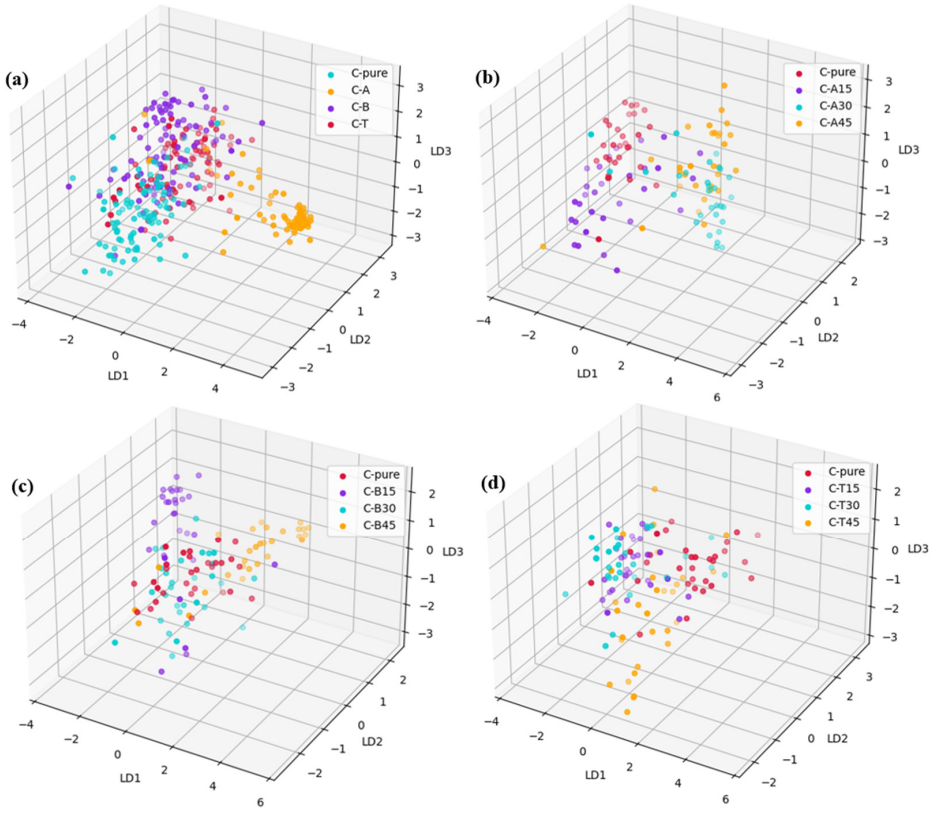


Figure 8. LDA results for different feature datasets extracted from the original response image: (**a**) *I*; (**b**) *I-ca*; (**c**) *I-cb*; (**d**) *I-ct*.

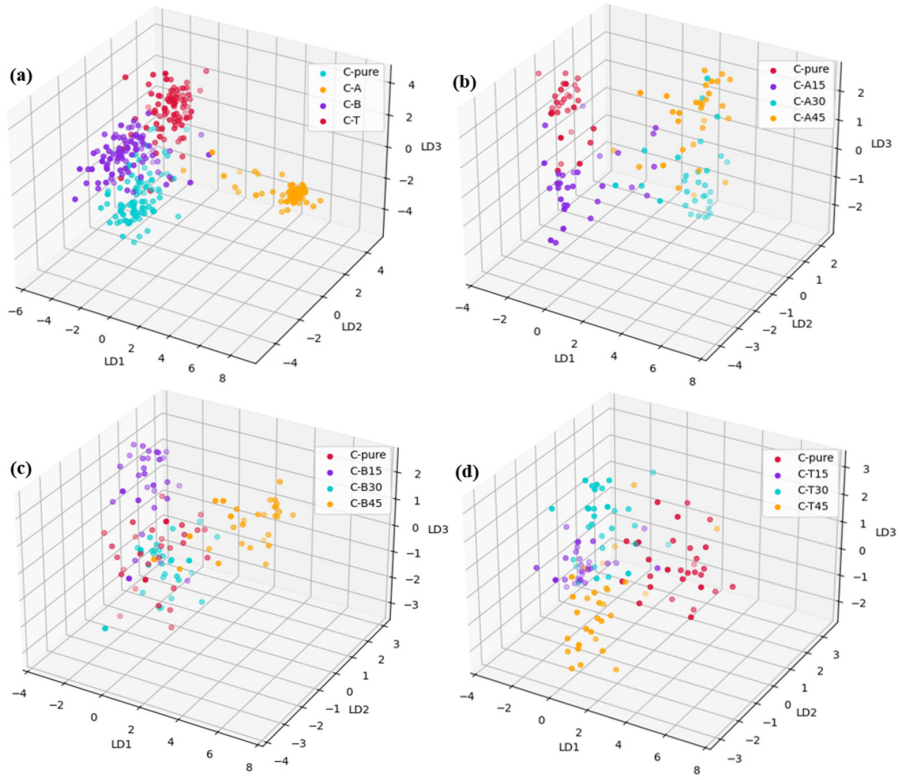


Figure 9. LDA results for different HOG feature datasets: (**a**) *H*; (**b**) *H-ca*; (**c**) *H-cb*; (**d**) *H-ct*.

5.2. SVM Classification Results

In this paper, the grid search method was used to search the optimal parameters of the HOG and SVM parameters, and the mean value of the identification accuracies of the 5-fold cross-validation was employed to evaluate these parameters. In terms of the HOG parameters, the cell size was set as 4, 6, 8, 10, and 12, and block sizes were 1, 2, 3, and 4. The used kernel functions of SVM were linear, polynomial, sigmoid, and radial basis functions (RBF). The log2(C) and log2(γ) were set in the range of $[-10, 10]$ with the interval of 0.5. The best experimental results are summarized in Table 3. For the listed results, it should be noted when the same identification accuracy was obtained for the different combinations of HOG parameters, those parameters leading to the feature dataset with the smallest size were regarded as the best combination. According to the results, it seems that RBF performs best among all the kernel functions except on the dataset *I-ca*, for which the sigmoid function obtained the highest mean accuracy of 94.2%. It can also be seen that the proposed approach could achieve a satisfactory identification accuracy for different categories of adulterants, which is up to 98.3%. The identification accuracy of different adulterant content is slightly lower than that of category identification, but all the mean values of these were higher than 93%.

Figure 10 shows the mean identification accuracies of the SVM identification mode based on the original response data, image, and HOG features. The results also displayed the similar trend that the three types of features obtain higher accuracy for the identification of the adulterant categories than the content identification. The identification accuracies based on the original response data are 86.6%, 84.2%, 83.6%, and 81.6% corresponding to the adulterants categories, CA-content, CB-content, and CT-content respectively, which are relatively better compared with the results for original features (8.3%, 72.5%, 73.3%, and 70.0%, respectively). It should be noted that the identification accuracies for all the HOG features on both category and content identification are significantly higher than the other two types of feature datasets. It can therefore be concluded that although the identification result of the response image is lower than its corresponding initial response data, the proposed HOG feature extraction algorithm can mine odor features that contribute more to adulterant identification. This is because HOG could extract the key image features that are beneficial for identification and discard the weaker features and the noise information.

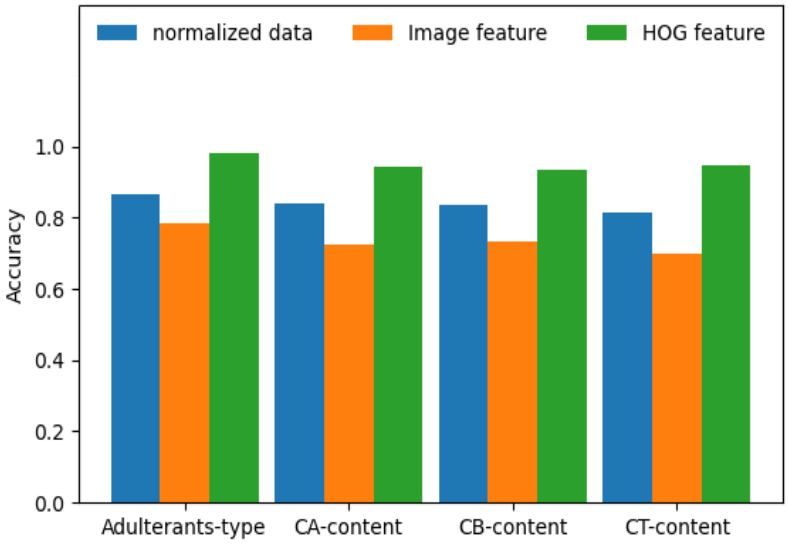


Figure 10. SVM identification accuracies based on different feature datasets.

Table 3. Summary of the identification accuracy based on HOG features with different parameters.

Datasets	HOG		SVM			Accuracy	Std
	Cell Size	Block Size	Kernel Functions	C	γ		
I	10	1	RBF	32.0	0.031	0.983	0.0136
I-ca	8	2	Sigmoid	2.0	2.0	0.942	0.0204
I-cb	12	1	RBF	0.125	8.0	0.933	0.0333
I-ct	4	1	RBF	11.314	90.510	0.950	0.0486

5.3. AlexNet Identification Results

Figure 11 is the AlexNet architecture investigated in this paper, which contains five convolutional layers (Cov), three max pooling layers (Max pooling), two fully connected layers (Fully connected), and an output layer [41]. Relu was used as the activation function to prevent the problem of gradient vanishing in this network. The max pooling layers were connected after Cov1, Cov2, and Cov5, and LRN (local response normalization) was set after the layers Cov1 and Cov2. Each of two fully connected layers has 4096 neurons and randomly deactivates neurons using the dropout method for reducing the overfitting [42,43]. The output layer contains four neurons and is used to represent the four categories or the four contents of the adulterations. In the current study, AlexNet network was implemented with the PyTorch (v1.13.0) deep-learning framework with the computer system configuration details shown in Table 4.

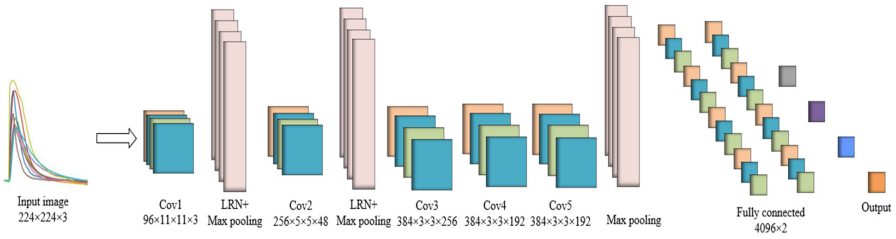


Figure 11. The architecture of AlexNet used to identify the adulterants in chili powder.

Table 4. Details of the system configuration for running AlexNet.

Item	Parameters
CPU	Core(TM) i9-12900H, 2.50 GHz
RAM	16.0 GB, 3200 MHz
GPU	NVIDIA GeForce RTX 3060 Laptop GPU 6 GB
Operating System	Windows 11

During the training of AlexNet, we randomly selected 80% samples from the feature dataset as the training sub-dataset, and the remaining 20% of samples were used as the testing sub-dataset. The size of the input image was resized to 224 × 224 pixels to match the input requirement of the AlexNet network. The Adam optimizer performs better in sparse data than the SGD optimizer due to it tending to fall into local optima. The Adam optimizer can assign different learning rates to different parameters, thus increasing the optimization speed. It therefore was chosen to be employed in the current study. The parameters of the training process are listed in Table 5.

Table 5. Parameters that were used during AlexNet training.

Configuration	Parameters
Input Image	224 × 224 Pixels, PNG
Epoch	300
Batch Size	2
Optimizer	Adam (adaptive moment estimation)
Learning Rate	0.0002

Figure 12 shows the performance comparison of the AlexNet training process on different datasets. It can be seen that the best performance was obtained on the dataset *I* with the accuracy of 96.5%, and the slightly lower accuracies of 92.7%, 94.7%, and 93.7% were run on the other three datasets *I-ca*, *I-cb*, and *I-ct*. The model parameters that obtained the highest accuracy on each training dataset were also validated on each corresponding testing sub-dataset. Table 6 shows the comparison of the identification accuracies of HOG+SVM and AlexNet. It can be seen HOG+SVM obtained the absolute higher identification accuracy than AlexNet on all datasets, as the identification accuracy of the deep-learning algorithm is highly dependent on the amount of training data. If the number of samples increased, AlexNet should express higher identification accuracy. However, the time consumed for both training and identification process will undoubtedly be lengthened. Furthermore, collecting more sample data also requires a lot of time. It should be noted that due to the sample number of the dataset *I* being much greater than other datasets, the training on the dataset *I* inevitably takes the longest time. There is a growing demand for the E-nose to be miniaturized and portable in recent years; the HOG+SVM approach is therefore easier to deploy on portable devices than neural network models such as AlexNet.

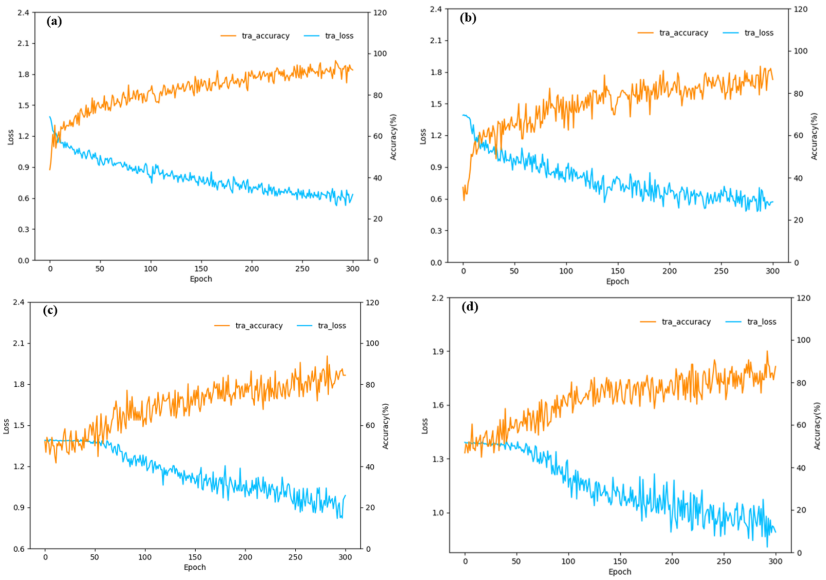


Figure 12. Performance of the AlexNet training process on different datasets: (**a**) *I*; (**b**) *I-ca*; (**c**) *I-cb*; (**d**) *I-ct*.

Table 6. Comparison of the identification accuracies of the model HOG+SVM and AlexNet.

Datasets	Identification Accuracy		Identification Time	
	HOG+SVM	AlexNet	HOG+SVM	AlexNet
I	98.3%	91.6%	7.24 s	11.36 s
I-ca	94.2%	83.3%	3.50 s	5.06 s
I-cb	93.3%	79.16%	3.52 s	5.58 s
I-ct	95.0%	87.50%	4.12 s	5.13 s

6. Conclusions

In this paper, the identification of the categories and contents of different adulterants in chili powder was successfully realized by using an E-nose system and the HOG feature extraction algorithm combined with an SVM identification model. The main results are as follows:

(1) Extracting odor features using the HOG algorithm could increase the distinguishability of the features, which is beneficial for subsequent pattern recognition;

(2) Efficient identification of the adulterant could be better realized by using the as-proposed HOG+SVM approach than with a neural network model such as AlexNet;
(3) The identification of adulterant content is relatively more difficult than the category identification, which may be solved by improving the performance of the E-nose system.

Author Contributions: Conceptualization, Y.Z. (Yongli Zhao); methodology, P.P. and Y.Z. (Yongli Zhao); software, P.P.; validation, P.P., F.B., Y.Z. (Yafei Zhang) and F.J.; formal analysis, P.P.; investigation, Y.Z. (Yafei Zhang); resources, data curation, P.P., F.B. and Y.Z. (Yafei Zhang); writing—original draft, P.P.; writing—review and editing, P.P.; visualization, Y.Z. (Yafei Zhang) and F.J.; supervision, Y.Z. (Yongli Zhao). All authors have read and agreed to the published version of the manuscript.

Funding: This research received no external funding.

Institutional Review Board Statement: Not applicable.

Informed Consent Statement: Not applicable.

Data Availability Statement: Data are contained within the article.

Conflicts of Interest: The authors declare no conflicts of interest.

References

1. Johnson, J.B.; Mani, J.S.; Walsh, K.B.; Naiker, M. Infrared spectroscopy for the quality assessment of habanero chilli: A proof-of-concept study. *Food Meas.* **2023**, *17*, 1764–1774. [CrossRef]
2. Rollyson, W.D.; Stover, C.A.; Brown, K.C.; Perry, H.E.; Stevenson, C.D.; McNees, C.A.; Ball, J.G.; Valentovic, M.A.; Dasgupta, P. Bioavailability of capsaicin and its implications for drug delivery. *J. Control. Release* **2014**, *196*, 96–105. [CrossRef] [PubMed]
3. Baenas, N.; Belović, M.; Ilic, N.; Moreno, D.A.; García-Viguera, C. Industrial use of pepper (*Capsicum annum* L.) derived products: Technological benefits and biological advantages. *Food Chem.* **2019**, *274*, 872–885. [CrossRef] [PubMed]
4. Genualdi, S.; MacMahon, S.; Robbins, K.; Farris, S.; Shyong, N.; DeJager, L. Method development and survey of Sudan I–IV in palm oil and chilli spices in the Washington, DC, area. *Food Addit. Contam. Part A Chem.* **2016**, *33*, 583–591. [CrossRef] [PubMed]
5. Monago-Maraña, O.; Eskildsen, C.E.; de la Peña, A.M.; Galeano-Díaz, T.; Wold, J.P. Non-destructive fluorescence spectroscopy combined with second-order calibration as a new strategy for the analysis of the illegal Sudan I dye in paprika powder. *Microchem. J.* **2020**, *154*, 104539. [CrossRef]
6. Monago-Maraña, O.; Eskildsen, C.E.; Afseth, N.K.; Galeano-Díaz, T.; de la Peña, A.M.; Wold, J.P. Non-destructive Raman spectroscopy as a tool for measuring ASTA color values and Sudan I content in paprika powder. *Food Chem.* **2019**, *274*, 187–193. [CrossRef]
7. Sarkar, T.; Choudhury, T.; Bansal, N.; Arunachalaeshwaran, V.R.; Khayrullin, M.; Shariati, M.A.; Lorenzo, J.M. Artificial Intelligence Aided Adulteration Detection and Quantification for Red Chilli Powder. *Food Anal. Methods* **2023**, *16*, 721–748. [CrossRef]
8. Galvin-King, P.; Haughey, S.A.; Elliott, C.T. Herb and spice fraud; the drivers, challenges and detection. *Food Control* **2018**, *88*, 85–97. [CrossRef]
9. Dhanya, K.; Syamkumar, S.; Siju, S.; Sasikumar, B. SCAR markers for adulterant detection in ground chilli. *Br. Food J.* **2011**, *113*, 656–668. [CrossRef]
10. Ndlovu, P.F.; Magwaza, L.S.; Tesfay, S.Z.; Mphahlele, R.R. Destructive and rapid non-invasive methods used to detect adulteration of dried powdered horticultural products: A review. *Food Res. Int.* **2022**, *157*, 111198. [CrossRef]
11. Oliveira, M.M.; Cruz-Tirado, J.P.; Barbin, D.F. Nontargeted analytical methods as a powerful tool for the authentication of spices and herbs: A review. *Compr. Rev. Food. Sci. Food Saf.* **2019**, *18*, 670–689. [CrossRef] [PubMed]
12. Khan, M.H.; Saleem, Z.; Ahmad, M.; Sohaib, A.; Ayaz, H.; Mazzara, M.; Raza, R.A. Hyperspectral imaging-based unsupervised adulterated red chili content transformation for classification: Identification of red chili adulterants. *Neural Comput. Appl.* **2021**, *33*, 14507–14521. [CrossRef]
13. Peng, Z.; Zhao, Y.; Yin, J.; Peng, P.; Ba, F.; Liu, X.; Guo, Y.; Rong, Q.; Zhang, Y. A Comprehensive Evaluation Model for Optimizing the Sensor Array of Electronic Nose. *Appl. Sci.* **2023**, *13*, 2338. [CrossRef]
14. Modupalli, N.; Naik, M.; Sunil, C.K.; Natarajan, V. Emerging non-destructive methods for quality and safety monitoring of spices. *Trends Food Sci. Technol.* **2021**, *108*, 133–147. [CrossRef]
15. Chilo, J.; Pelegri-Sebastia, J.; Cupane, M.; Sogorb, T. E-nose application to food industry production. *IEEE Instrum. Meas. Mag.* **2016**, *19*, 27–33. [CrossRef]
16. Tan, J.; Xu, J. Applications of electronic nose (e-nose) and electronic tongue (e-tongue) in food quality-related properties determination: A review. *Artif. Intell. Agric.* **2020**, *4*, 104–115. [CrossRef]
17. Liu, H.; Zeng, F.; Wang, Q.; Ou, S.; Tan, L.; Gu, F. The effect of cryogenic grinding and hammer milling on the flavour quality of ground pepper (*Piper nigrum* L.). *Food Chem.* **2013**, *141*, 3402–3408. [CrossRef]

18. Wen, J.; Zhao, Y.; Rong, Q.; Yang, Z.; Yin, J.; Peng, Z. Rapid odor recognition based on relief algorithm using electronic nose and its application in fruit identification and classification. *J. Food Meas. Charact.* **2022**, *16*, 2422–2433. [CrossRef]
19. Heidarbeigi, K.; Mohtasebi, S.S.; Foroughirad, A.; Ghasemi-Varnamkhasti, M.; Rafiee, S.; Rezaei, K. Detection of adulteration in saffron samples using electronic nose. *Int. J. Food Prop.* **2015**, *18*, 1391–1401. [CrossRef]
20. Jia, P.; Huang, T.; Wang, L.; Duan, S.; Yan, J.; Wang, L. A novel pre-processing technique for original feature matrix of electronic nose based on supervised locality preserving projections. *Sensors* **2016**, *16*, 1019. [CrossRef]
21. Noh, H.W.; Jang, Y.; Park, H.D.; Kim, D.; Choi, J.H.; Ahn, C.G. A selective feature optimized multi-sensor based e-nose system detecting illegal drugs validated in diverse laboratory conditions. *Sens. Actuator B Chem.* **2023**, *390*, 133965. [CrossRef]
22. Kalidoss, R.; Umapathy, S.; Thirunavukkarasu, U.R. A breathalyzer for the assessment of chronic kidney disease patients' breathprint: Breath flow dynamic simulation on the measurement chamber and experimental investigation. *Biomed. Signal Process. Control* **2021**, *70*, 103060. [CrossRef]
23. Wang, Z.; Chen, W.; Gu, S.; Wang, Y.; Wang, J. Evaluation of trunk borer infestation duration using MOS E-nose combined with different feature extraction methods and GS-SVM. *Comput. Electron. Agric.* **2020**, *170*, 105293. [CrossRef]
24. Yin, J.; Zhao, Y.; Peng, Z.; Ba, F.; Peng, P.; Liu, X.; Rong, Q.; Guo, Y.; Zhang, Y. Rapid Identification Method for CH_4/CO/CH_4-CO Gas Mixtures Based on Electronic Nose. *Sensors* **2023**, *23*, 2975. [CrossRef]
25. Rahimzadeh, H.; Sadeghi, M.; Ghasemi-Varnamkhasti, M.; Mireei, S.A.; Tohidi, M. On the feasibility of metal oxide gas sensor based electronic nose software modification to characterize rice ageing during storage. *J. Food Eng.* **2019**, *245*, 1–10. [CrossRef]
26. Chen, D.; Wang, B.; Zhang, T.; Chang, Z. Towards accuracy recognition and content estimation of typical pesticides in groundwater via electronic nose. *Sens. Actuator A Phys.* **2023**, *362*, 114642. [CrossRef]
27. Chen, K.; Liu, L.; Nie, B.; Lu, B.; Fu, L.; He, Z.; Li, W.; Pi, X.; Liu, H. Recognizing lung cancer and stages using a self-developed electronic nose system. *Comput. Biol. Med.* **2021**, *131*, 104294. [CrossRef]
28. Han, L.; Chen, M.; Li, Y.; Wu, S.; Zhang, L.; Tu, K.; Pan, L.; Wu, J.; Song, L. Discrimination of different oil types and adulterated safflower seed oil based on electronic nose combined with gas chromatography-ion mobility spectrometry. *J. Food Compos. Anal.* **2022**, *114*, 104804. [CrossRef]
29. Yan, J.; Guo, X.; Duan, S.; Jia, P.; Wang, L.; Peng, C.; Zhang, S. Electronic nose feature extraction methods: A review. *Sensors* **2015**, *15*, 27804–27831. [CrossRef]
30. Avian, C.; Mahali, M.I.; Putro, N.A.S.; Prakosa, S.W.; Leu, J.S. Fx-Net and PureNet: Convolutional Neural Network architecture for discrimination of Chronic Obstructive Pulmonary Disease from smokers and healthy subjects through electronic nose signals. *Comput. Biol. Med.* **2022**, *148*, 105913. [CrossRef]
31. Shi, Y.; Wang, B.; Yin, C.; Li, Z.; Yu, Y. Performance improvement: A lightweight gas information classification method combined with an electronic nose system. *Sens. Actuator B Chem.* **2023**, *396*, 134551. [CrossRef]
32. Zhang, Q.; Kang, S.; Yin, C.; Li, Z.; Shi, Y. An adaptive learning method for the fusion information of electronic nose and hyperspectral system to identify the egg quality. *Sens. Actuator A Phys.* **2022**, *346*, 113824. [CrossRef]
33. Zhao, Y.; Wang, Y.; Peyraut, F.; Planche, M.; Ilavsky, J.; Liao, H.; Montavon, G.; Lasalle, A.; Allimant, A. Parametric Analysis and Modeling for the Porosity Prediction in Suspension Plasma-Sprayed Coatings. *J. Therm. Spray Technol.* **2020**, *29*, 51–59. [CrossRef]
34. Kapoor, R.; Gupta, R.; Jha, S.; Kumar, R. Detection of power quality event using histogram of oriented gradients and support vector machine. *Measurement* **2018**, *120*, 52–75. [CrossRef]
35. Tomar, D.; Agarwal, S. Twin Support Vector Machine: A review from 2007 to 2014. *Egypt. Inform. J.* **2015**, *16*, 55–69. [CrossRef]
36. Ba, F.; Peng, P.; Zhang, Y.; Zhao, Y. Classification and Identification of Contaminants in Recyclable Containers Based on a Recursive Feature Elimination-Light Gradient Boosting Machine Algorithm Using an Electronic Nose. *Micromachines* **2023**, *14*, 2047. [CrossRef]
37. Zhao, Y.L.; Zhao, C.H.; Huang, J.; Zhao, B. LaMnO3–Ni0.75Mn2.25O4 Supported Bilayer NTC Thermistors. *J. Am. Ceram. Soc.* **2014**, *97*, 1016–1019. [CrossRef]
38. John Lu, Z.Q. The Elements of Statistical Learning: Data Mining, Inference, and Prediction. *J. R. Stat. Soc. Ser. A Stat. Soc.* **2010**, *173*, 693–694. [CrossRef]
39. Mahmodi, K.; Mostafaei, M.; Mirzaee-Ghaleh, E. Detection and classification of diesel-biodiesel blends by LDA, QDA and SVM approaches using an electronic nose. *Fuel* **2019**, *258*, 116114. [CrossRef]
40. Anwar, H.; Anwar, T.; Murtaza, S. Review on food quality assessment using machine learning and electronic nose system. *Biosens. Bioelectron. X* **2023**, *14*, 100365. [CrossRef]
41. Krizhevsky, A.; Sutskever, I.; Hinton, G.E. Imagenet Classification with Deep Convolutional Neural Networks. *Neural Inf. Process. Syst.* **2012**, *25*, 84–90. [CrossRef]
42. Simonyan, K.; Zisserman, A. Very deep convolutional networks for large-scale image recognition. *arXiv* **2014**, arXiv:1409.1556. [CrossRef]
43. Urbaniak, I.; Wolter, M. Quality assessment of compressed and resized medical images based on pattern recognition using a convolutional neural network. *Commun. Nonlinear Sci. Numer. Simul.* **2021**, *95*, 105582. [CrossRef]

Disclaimer/Publisher's Note: The statements, opinions and data contained in all publications are solely those of the individual author(s) and contributor(s) and not of MDPI and/or the editor(s). MDPI and/or the editor(s) disclaim responsibility for any injury to people or property resulting from any ideas, methods, instructions or products referred to in the content.